PNAS
www.pnas.org

Supplementary Information for

Mechanism of the E2 to E1 transition in Ca^{2+}-pump revealed by crystal structures of gating residue mutants

Naoki Tsunekawa, Haruo Ogawa, Junko Tsueda, Toshihiko Akiba and Chikashi Toyoshima

Chikashi Toyoshima
Email: ct@iam.u-tokyo.ac.jp

This PDF file includes:

Supplementary text
Figs. S1 to S10
Tables S1 to S3
Captions for movies S1 to S3
References for SI reference citations

Other supplementary materials for this manuscript include the following:

Movies S1 to S3

www.pnas.org/cgi/doi/10.1073/pnas.1815472115

Supplementary Information Text

Materials and Methods

Construction, expression and purification of SERCA1a mutants. Site-directed mutageneses were introduced by inverse polymerase chain reaction. pFN21K vector (Promega), which carries a part of pIRES2-SERCA1a (1) including IRES and AcGFP, was used as the template. Mutations were confirmed by DNA sequencing. HaloTag-fused SERCA1a mutants were subcloned into pShuttle-CMV vector (Stratagene). AdEasy XL adenoviral vector system (Stratagene) was used to establish recombinant adenovirus. Production and purification of SERCA1a mutants were carried out as described previously (1)

Crystallization. For Glu309Ala(TG) crystals, protein solution contained 4 mg/ml affinity purified ATPase, 3.2 mg/ml phosphatidylcholine, 0.71% $C_{12}E_8$, 20% glycerol, 1 mM $CaCl_2$, 1 mM $MgCl_2$, 5 mM EGTA, 0.06 mM thapsigargin (TG), 0.24 mM 2,5-di(*tert*-butyl)-1,4-benzo-hydroquinone (BHQ) and 20 mM MOPS, pH 7.0. The reservoir consisted of 16% glycerol, 16% PEG1000, 2.5 mM NaN_3, 1 mM $MgCl_2$, 3 mM EGTA, 40 mM $MgSO_4$, 20 mM Na acetate and 40 mM MES, pH 6.1. Two µl each of protein and reservoir solutions were mixed for hanging drop crystallization at 20°C. For Glu309Gln(TG) crystals, protein solution contained 3 mg/ml affinity purified ATPase, 1.8 mg/ml phosphatidylcholine, 0.32% $C_{12}E_8$, 20% glycerol, 1 mM $CaCl_2$, 1 mM $MgSO_4$, 3 mM EGTA, 0.03 mM TG, and 20 mM MOPS, pH 7.0. The reservoir consisted of 16% glycerol, 16-18% PEG2000, 2.5 mM NaN_3, 1 mM $MgSO_4$, 1 mM EGTA, 0.15% decylmaltoside and 40 mM MES, pH 6.1. 0.2 µl each of protein and reservoir solutions were mixed using Mosquito (TTP Labtech) for sitting drop crystallization at 20°C.

Data collection and structure determination. Diffraction data were collected from the crystals cooled to 100 K at BL41XU of SPring-8 using Rayonix MX225HE CCD detector. The wavelength used was 0.9 Å. All data were processed with Denzo and Scalepack (2). Diffraction data from the two best crystals were averaged. Crystal structures were determined by molecular replacement starting from a model for the E2 state of native SERCA1a (PDB ID: 2AGV) (3) using CNS (4). The atomic models were refined using CNS with restraints on hydrogen bonds (5) and finally with Phenix (6). Domain movements were analysed with Dyndom (7). Structure figures were prepared with TurboFRODO, Molscript (8) and PyMol (The PyMOL Molecular Graphics System, Schrödinger LLC).

Quantum chemical refinement of atomic models. The atomic model examined by quantum chemical calculations using density functional theory (DFT) consists of 58 residues on four transmembrane helices selected to retain the environment of Glu/Gln309 (Table S3). To minimize computation time, the side chains of the residues on the periphery of the system and facing the outside were reduced to Cβ. Hydrogen atoms were added by psfgen in NAMD (9). All the carboxyl groups in the acidic residues included in the system, namely, Glu309, Glu771, and Asp800, were protonated following the prediction by Propka (10). The N- and C-termini of each helix were capped with an acetyl group and N-methylamide, respectively. Altogether 843 atoms were included in the model for native ATPase and 844 in that for Glu309Gln.

The locations of H/H^+ were optimized first by DFT to the "Loose" level in g09 (11) at B3LYP/6-31G(d,p) (12-14) fixing all covalent dihedral angles. Then, the locations of all atoms were optimized to the "Default" level by DFT-D at B3LYP/6-31+G(d,p), in which the diffuse function (15) was excluded for carbon and Grimme's empirical dispersion correction (16) was included. Several restraints were imposed in the energy minimization (Table S3). For instance, seven heavy atoms were fixed in space in addition to all the Cα atoms except for those on the M4 helix; ten main chain dihedral angles at either end of M4 were fixed. Deviations of the optimized models from the originals were very small (Table S2). The minimization for the Glu309Ala mutant converged only to the "Loose" level.

Quantum chemical calculation of energy profile of hydrogen bond. To understand the Glu/Gln309 – Val304 hydrogen bonds, we examined two model systems, one of formic acid (HCOOH) and formaldehyde (CH_2O) to mimic Glu309-Val304, and the other of formamide ($HCONH_2$) and formaldehyde to mimic Gln309-Val304. The dispositions of non-hydrogen atoms were taken from the respective crystals structures. The atomic models were energy minimized by DFT-D at CAM-B3LYP/6-311++G(3df,2pd) (17) fixing the relative orientation of the two molecules (illustrated in Fig. S5). Then altogether 64 atomic models were generated for each system changing the distance from 2.5 to 8.0 Å and optimized in the same way. Finally, coupled cluster single-double and perturbative triple (CCSD(T)) calculations (18, 19) were carried out for each atomic model and the association energy of the two molecules was obtained with counterpoised correction for basis set superposition error (20, 21) (Fig. S5). These calculations show

that the optimal hydrogen bond distances are 2.83 and 3.16 Å for a protonated carboxyl-carbonyl and an amide-carbonyl, respectively.

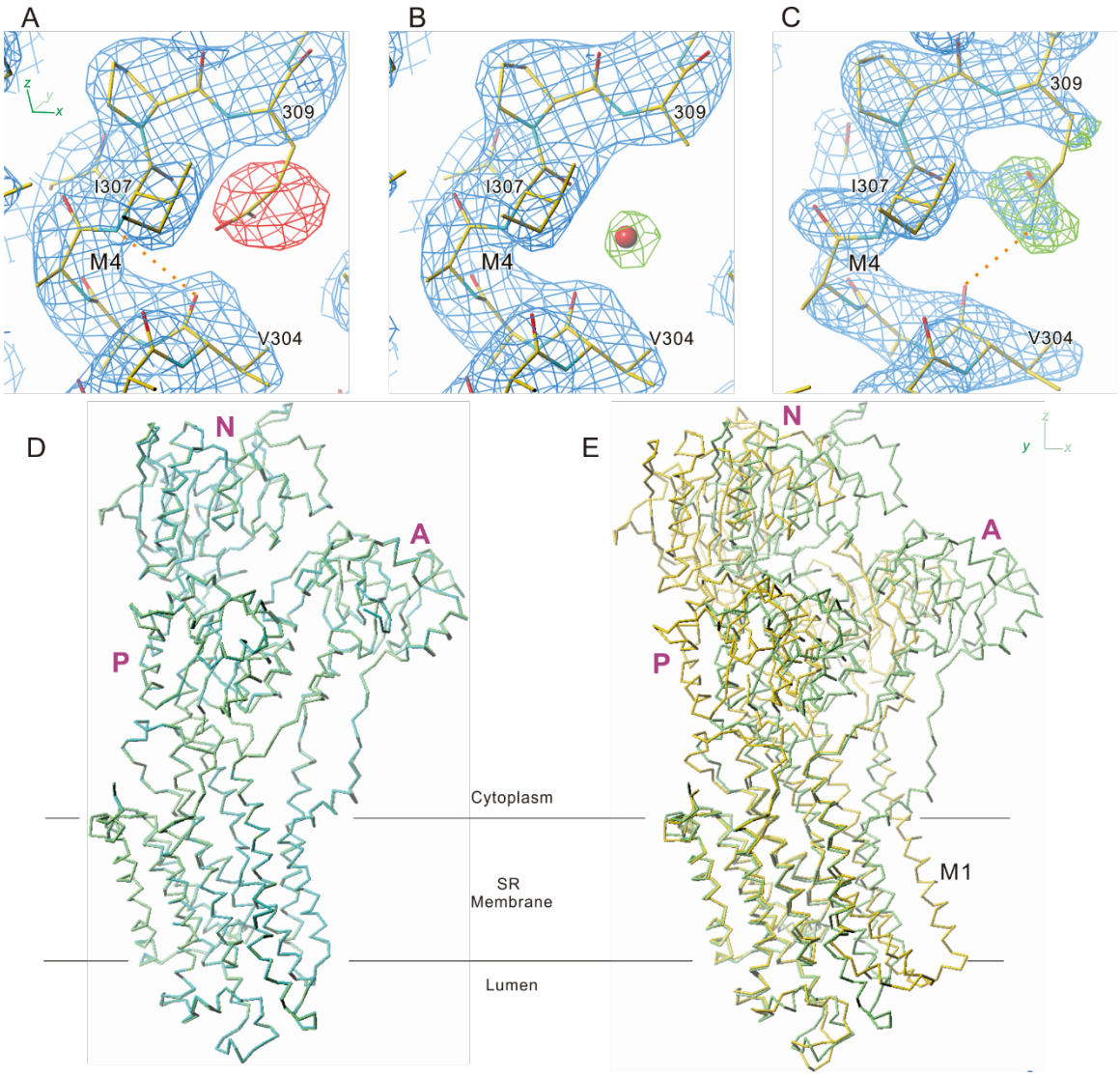

Fig. S1. Electron density maps of the mutant crystals around the substituted residue (Glu309) and overall structural changes due to the substitution of Glu309. (*A*, *B* and *C*) Electron density maps for the M4 helix around Glu309 in the Glu309Ala mutant (*A* and *B*) and in the Glu309Gln mutant (*C*), calculated assuming that Glu309 is not substituted in *A* but substituted with Ala in *B* and *C*. Blue nets represent 2 $|F_{obs}|$ - $|F_{calc}|$ maps contoured at 1.0σ (*A*, *B*). Red net represents negative density and the green one positive density at 3.5σ (*B*) or 3.0σ (*C*) in the $|F_{obs}|$ - $|F_{calc}|$ difference maps. Superimposed is the atomic model of native E2(TG). (*D* and *E*) Superimposition of the Cα trace of the native ATPase (cyan) and that of the Glu309Ala mutant (yellow, *D*) or Glu309Gln mutant (yellow, *E*). Three cytoplasmic domains are labeled (A, N and P). Thin horizontal lines approximate the boundary between the hydrophobic core of the bilayer and water. Val304 carbonyl is likely to be stabilized by a hydrogen bond (orange dotted line) with an

extra water molecule (small red sphere) in Glu309Ala (*B*) or with the side chain amide of Gln309 in Glu309Gln (*C*).

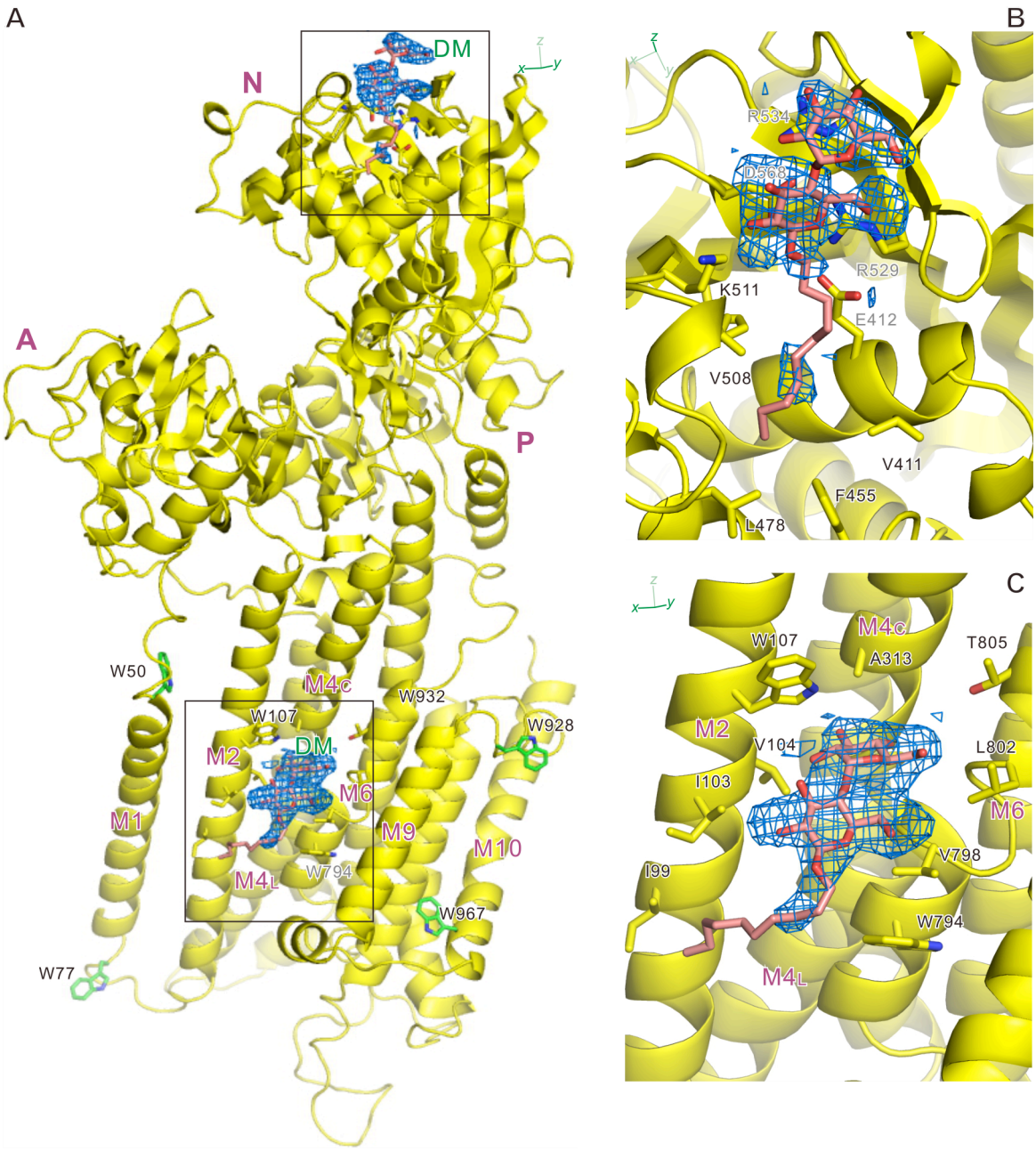

Fig. S2. Electron density maps of the Glu309Gln mutant crystal showing bound decylmaltoside (DM). (*A*) An overall view; (*B*) Details around the DM molecule in the N-domain; (*C*) Around the one in the transmembrane domain. Blue nets represent an omit annealed $|F_{obs}| - |F_{calc}|$ map contoured at 2σ. Several Trp side chains appear in green sticks (*A*), showing the positions of membrane-water interface (22).

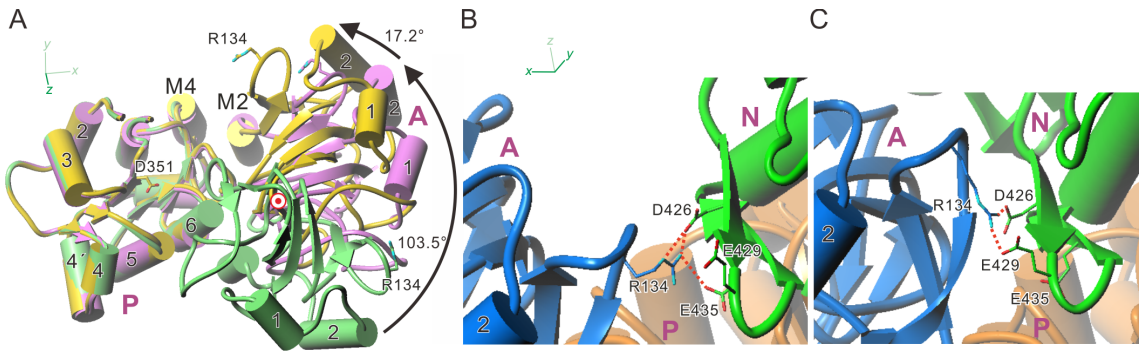

Fig. S3. Arrangement of the cytoplasmic domains and the A-domain – N-domain interface in different states. (*A*) Superimpositions of the A- and P-domains aligned with the P-domain. Colors used are yellow for the Glu309Gln mutant, violet for the native ATPase in E1·Mg^{2+} and lime for that in E2. The N-domain is removed for clarity. Viewed approximately perpendicular to the membrane. Double circle shows the position of the rotation axis of the A-domain. (*B* and *C*) Some details of the A-N interface at the periphery of the A domain in the Glu309Gln mutant (*B*) and in the native ATPase in E1·AMPPCP·2Ca^{2+} (*C*). Note that hydrogen bonding network (orange dotted lines) is formed in the mutant, implicating Arg134 (A), Asp426 and Glu435 (N) (*B*). Such a network is also observed in the crystal structure of E1·AMPPCP·2Ca^{2+} (*C*), in which Glu429 instead of Glu435 contributes (23). These residues have been subjects of mutagenesis studies (24, 25).

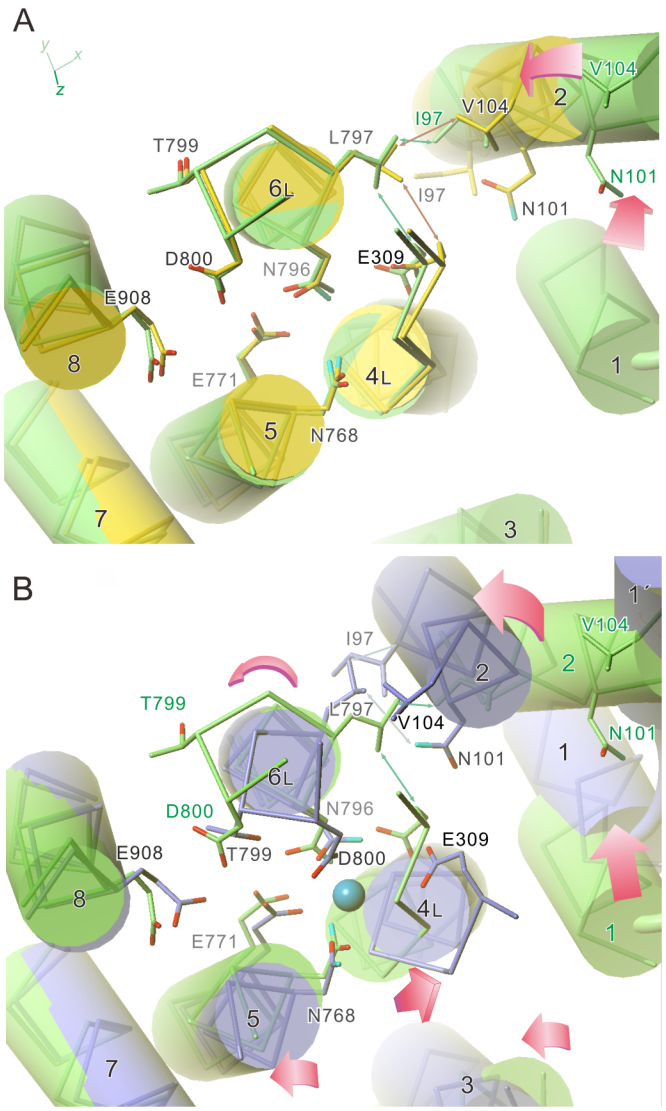

Fig. S4. Rearrangement of transmembrane helices. (*A*) Native E2 (lime) and E309Q mutant (yellow); (*B*) Native E2 (lime) and E1·Mg^{2+} (blue grey). Pink arrows show the movements required to realize the latter state from the former. Double headed arrows indicate van der Waals contacts involving Leu797, which is in contact in E2 with Ile97 (native) or Val104 (Glu309Gln) on M2 and Glu/Gln309 on M4 (*A*). Small cyan sphere in (*B*) represents bound Mg^{2+} in E1·Mg^{2+}.

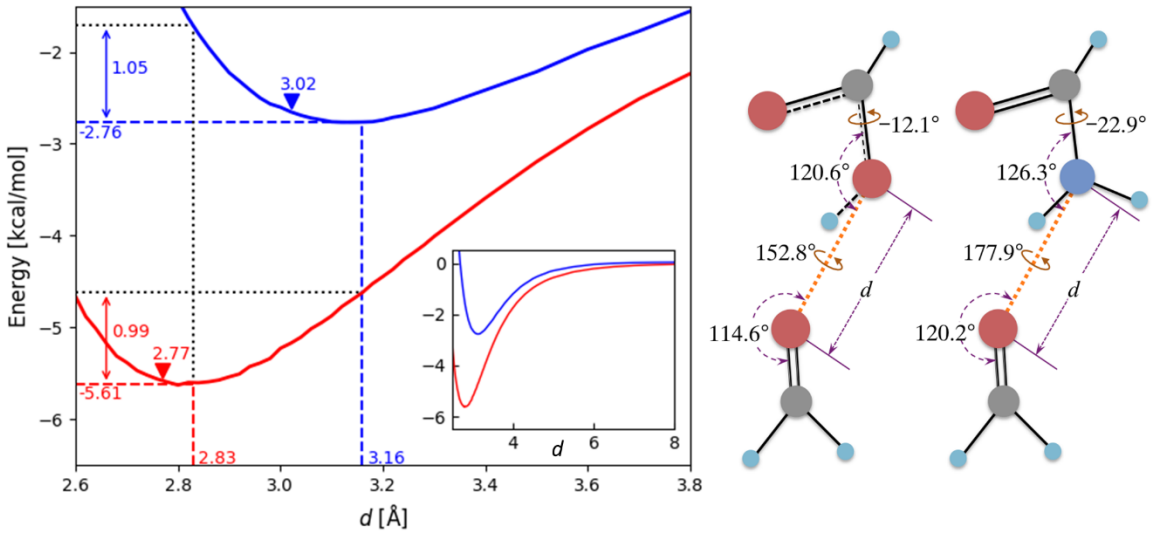

Fig. S5. Energy profiles of hydrogen bonds as a function of distance (*d*) between two heavy atoms working as hydrogen donor and acceptor. Calculated by CCSD(T) (18, 19) for a hydrogen bond between a protonated carboxyl and a carbonyl oxygen (red line) and that between an amide and a carbonyl oxygen (blue line), for which the minimum comes to 2.83 Å and 3.16 Å, respectively. The systems used for the calculations (right panel) reflect the dispositions of Glu/Gln309 and Val304 in the crystal structures. The arrowheads in the left panel indicate the distances in the relevant crystal structures. Inset shows the overall profiles.

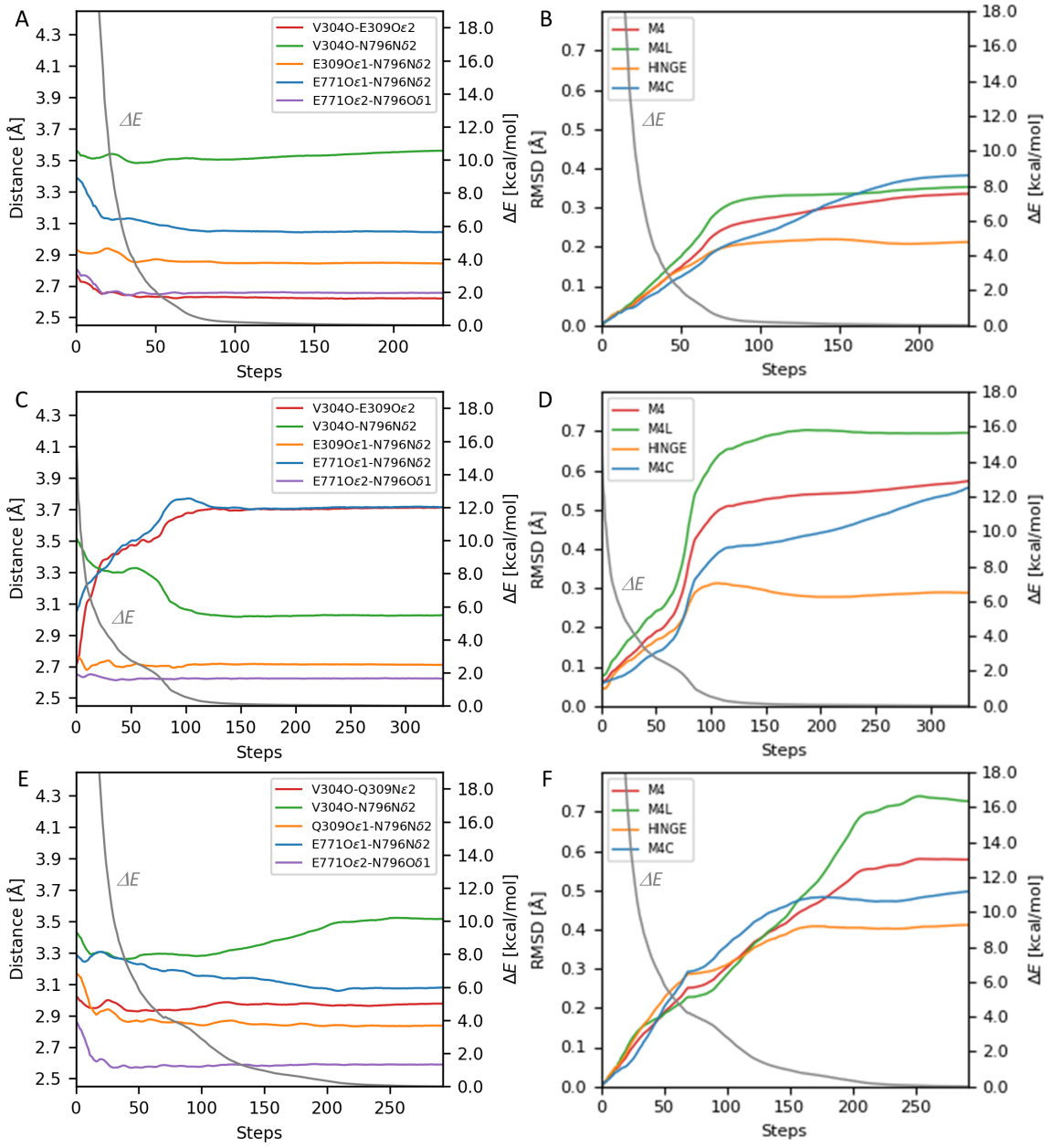

Fig. S6. Energy minimization by DFT-D of the atomic models of SERCA1a around Glu309. Changes in total energy (grey lines), distance between atoms of particular interest (left panels) and RMSD for Cα atoms (right panels) during the minimization. (*A* and *B*) Starting from the crystal structure of native ATPase. The Glu309 carboxyl is assumed to be protonated. (*C* and *D*) Glu309 in the energy minimized model (*A* and *B*) was deprotonated and subjected to energy minimization. (*E* and *F*) Starting from the Glu309Gln(TG) crystal structure. The colors used in the left panels are: red, Val304O-Glu309Oε2 (*A* and *C*) or Val304O-Gln309Nε2 (E); green, Val304O-Asn796Nδ2;

yellow, Glu309Oε1-Asn796Nδ2; blue, Glu771Oε1-Asn796Nδ2; purple, Glu771Oε2-Asn796Oδ1. In the right panels: red, all M4 (Ala301 to Pro312); green, M4L (Ala301 to Ala305); yellow, HINGE (Ala305 to Glu/Gln309); blue, M4C (Glu/Gln309 to Pro312).

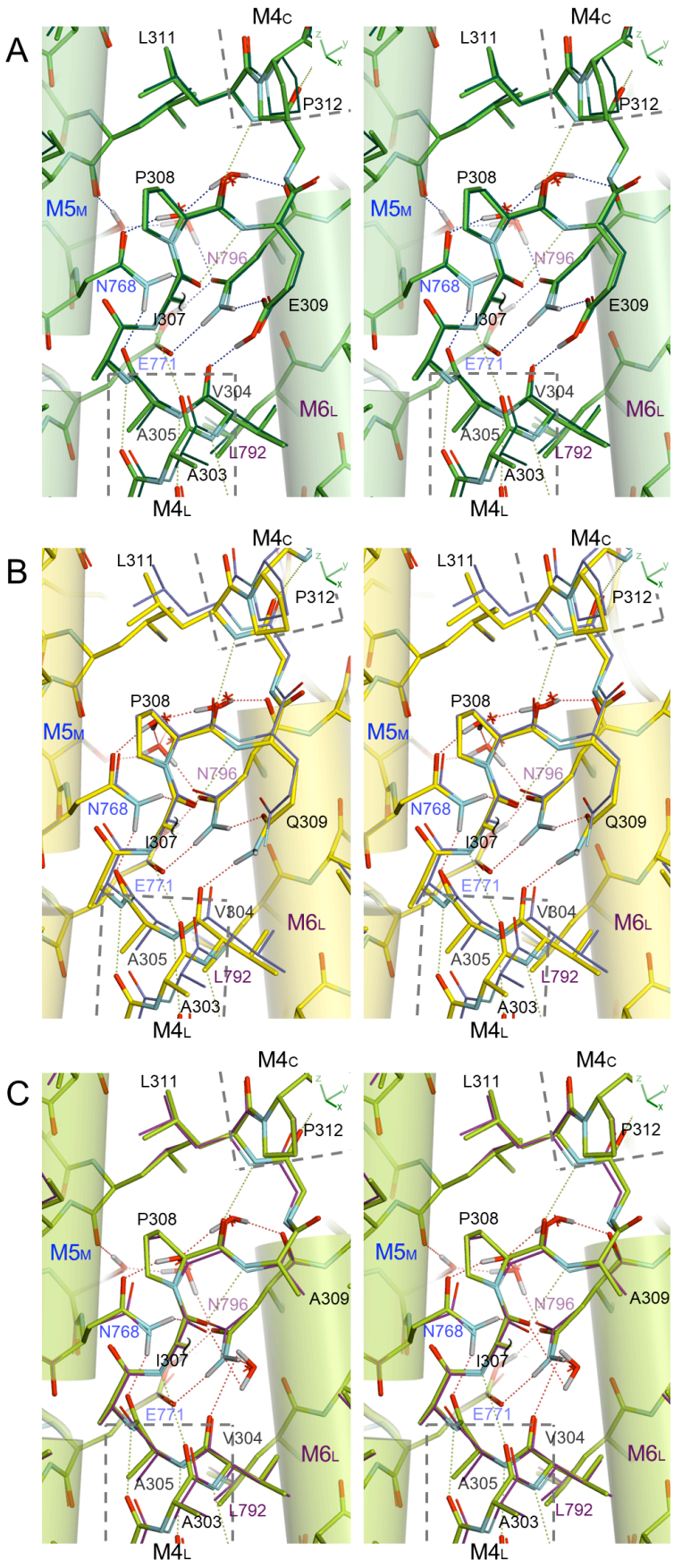

Fig. S7. Quantum chemically optimized atomic models of SERCA1a around

Glu309. (*A*) native ATPase in E2(TG) (a stereo version of Fig. 5*A*); (*B*) Glu309Gln mutant; (*C*) Glu309Ala mutant. Starting crystal structures appear as thin lines. Dotted lines represent hydrogen bonds (not exhaustive). The side chain of Ile307 is removed.

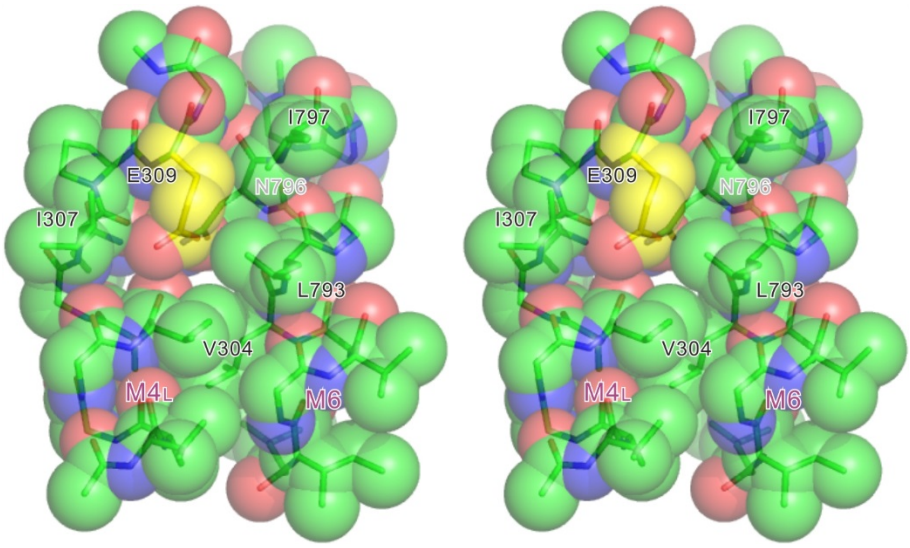

Fig. S8. Space-fill representation of the atomic model around the Glu309 side chain of SERCA1a in E2. A stereo picture of a view almost parallel to the membrane plane, showing tight contacts of the Glu309 side chain (carbon atoms in Glu309 appear yellow).

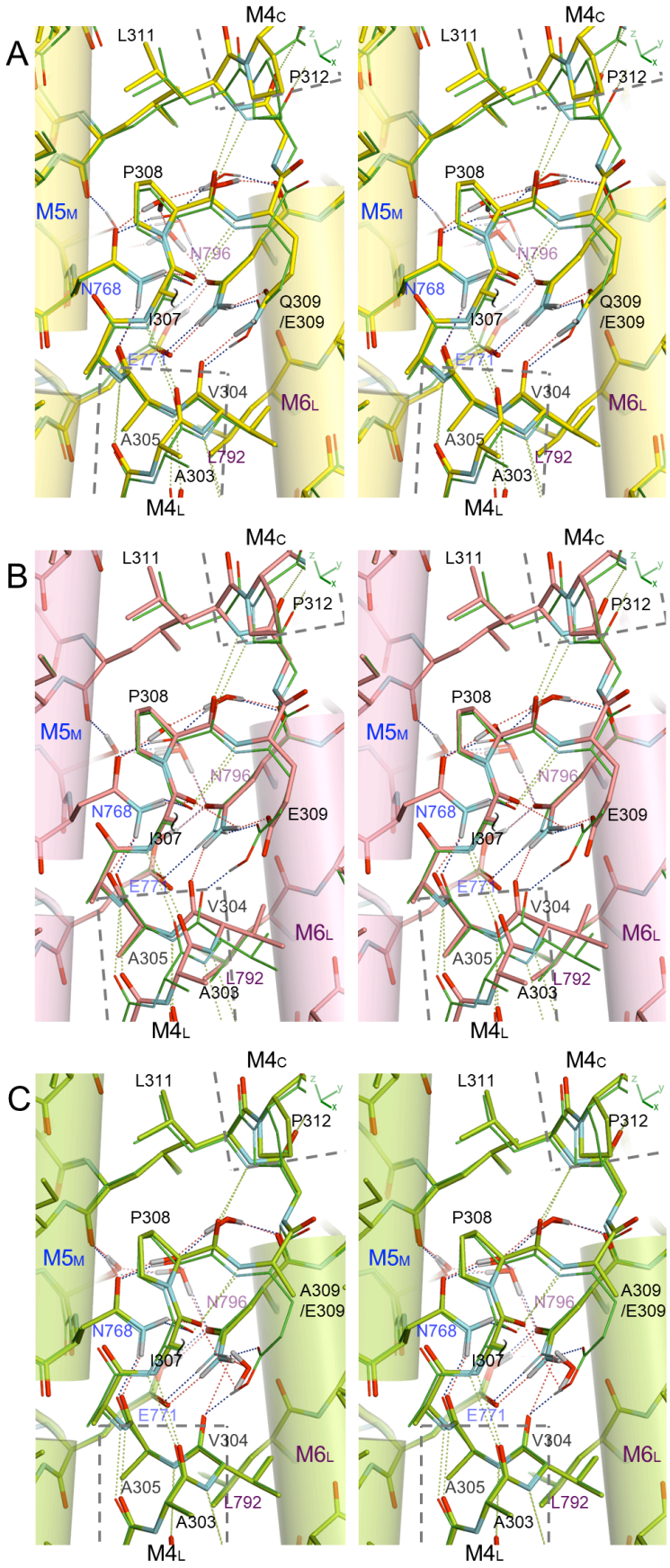

Fig. S9. Superimpositions of quantum chemically optimized atomic models of

SERCA1a in E2. Viewed parallel to the membrane in stereo. Those of Glu309Gln mutant (*A*, yellow sticks), native ATPase with deprotonated Glu309 (*B*, pink sticks) and Glu309Ala mutant (*C*, lime sticks) are superimposed with that of native ATPase with protonated Glu309 (thin green lines). Dotted lines represent hydrogen bonds. The side chain of Ile307 is removed for clarity. *A* and *B* are stereo versions of Fig. 5*B* and 5*C*, respectively.

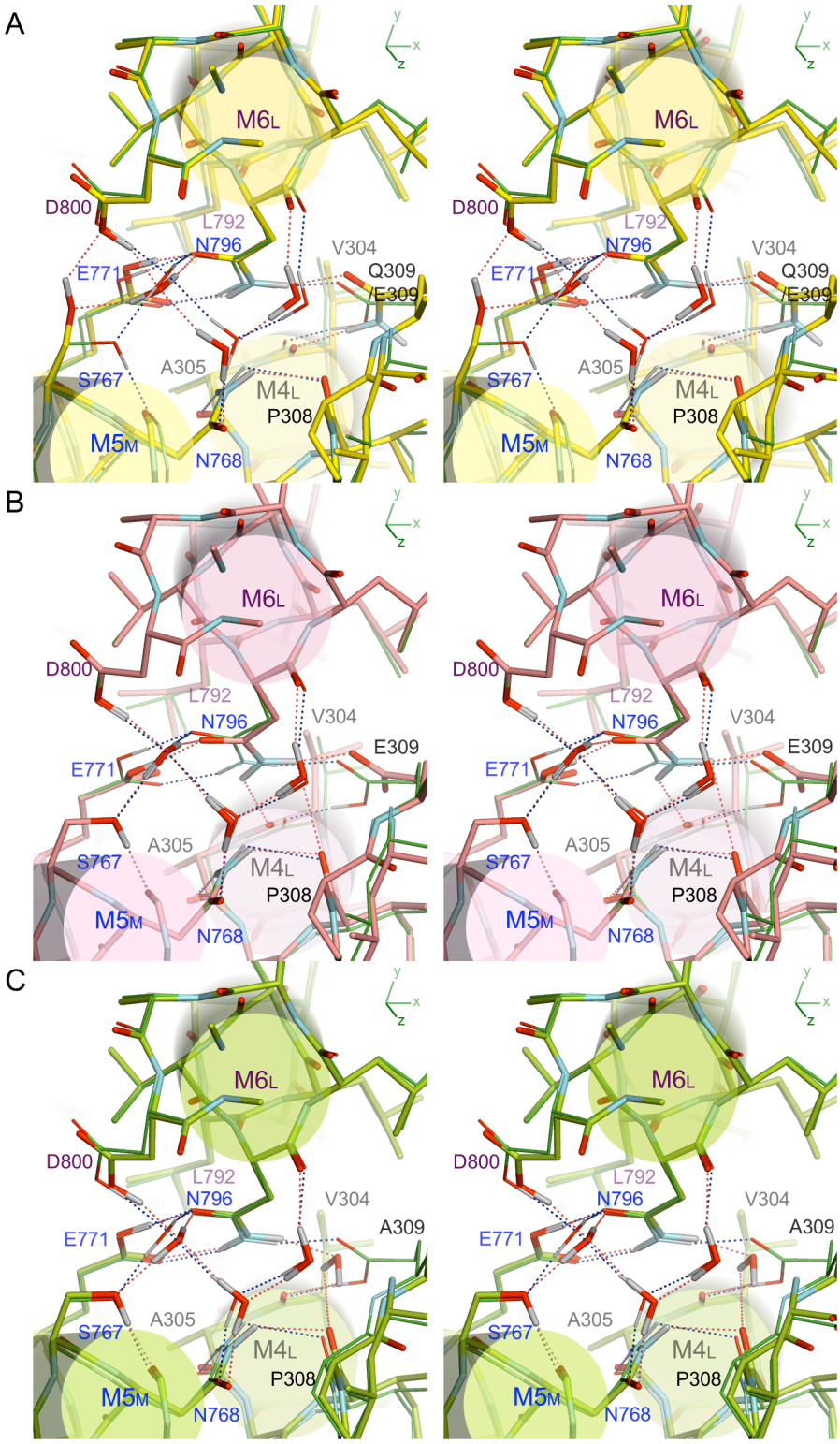

Fig. S10. Superimpositions of quantum chemically optimized atomic models of SERCA1a in E2. Viewed from the cytoplasmic side in stereo. Those of Glu309Gln mutant (*A*, yellow sticks), native ATPase with deprotonated Glu309 (*B*, pink sticks) and Glu309Ala mutant (*C*, lime sticks) are superimposed with that of native ATPase with protonated Glu309 (thin green lines). Dotted lines represent hydrogen bonds.

Table S1. Data collection and refinement statistics

	Glu309Ala(TG)	Glu309Gln(TG)
Data collection		
Space group	$P4_12_12$	$P2_12_12$
Cell dimensions		
a, *b*, *c* (Å)	71.2, 71.2, 589.2	261.0, 86.9, 60.2
α, β, γ (°)	90, 90, 90	90, 90, 90
Resolution (Å)	50-3.3 (3.41-3.30)	50-2.5 (2.58-2.50)
R_{sym} or R_{merge}	0.056 (0.233)	0.133 (0.609)
I/σ	15.0 (2.0)	13.9 (2.2)
Completeness (%)	99.0 (95.3)	98.5 (98.0)
Redundancy	14.4 (11.2)	8.7 (8.1)
No. of crystals	2	2
Refinement		
Resolution (Å)	16.0-3.3 (3.55–3.30)	16.0-2.5 (2.58-2.50)
No. reflections	23,965	47,627
$R_{work/}$ R_{free}	19.5/23.2	22.5/25.6
No. atoms		
Protein	7,701	7,709
Ligand/ion	6	5
Water	0	235
B-factors		
Protein	98.5	72.1
Ligand/ion	164.1	112.2
Water	-	52.5
RMSD		
Bond lengths (Å)	0.002	0.002
Bond angles (º)	0.445	0.452
Ramachandran plot (%) (Favored, allowed, generous, disallowed)	88.9, 11.1, 0.0, 0.0	88.9, 11.1, 0.0, 0.0

* Highest resolution shell is shown in parentheses.

Table S2. Distances between atoms of particular interest in the atomic models of native and Glu309Gln/Ala mutants of SERCA1a in E2(TG)

	native*	E309(+H^+)†	E309(-H^+)‡	E309Q*	Q309§	E309A*	A309¶	
V304O-I307N	3.68	3.76	3.45	3.91	3.53	3.74	3.64	[Å]
V304O-E309Oε2	2.77	2.62	3.71					
-Q309Nε2				3.02	2.98			
V304O-N796Nδ2	3.56	3.56	3.03	3.43	3.52	3.84	3.45	
A305O-N768Nδ2	2.76	2.82	2.84	2.96	2.83	3.14	2.86	
I307O-E/Q309Oε1	3.02	3.03	3.21	2.87	3.23			
I307O-E309Oε2	3.04	3.04	3.58					
-Q309Nε2				3.24	3.08			
E/Q309Oε1-N796Nδ2	2.93	2.84	2.71	3.17	2.84			
E771Oε1-N796Nδ2	3.39	3.04	3.71	3.29	3.08	2.99	3.13	
E771Oε2-N796Oδ1	2.81	2.66	2.62	2.86	2.59	2.78	2.63	

* crystal structure

† DFT optimized atomic model with protonated Glu309 derived from the crystal structure of native ATPase in E2(TG). RMSD from the starting model calculated for all unfixed non-hydrogen atoms was 0.23 Å

‡ DFT optimized model of native ATPase with deprotonated Glu309; derived from the atomic model "E309(+H^+)". RMSD: 0.30 Å

§ DFT optimized model of Glu309Gln derived from the crystal structure. RMSD: 0.39 Å

¶ DFT optimized model of the Glu309Ala mutant; derived from the crystal structure. RMSD: 0.27 Å

Underscores indicate hydrogen bonds (the distance between a donor and an acceptor is equal or less than 3.5 Å, and the angle spanned by the acceptor, donor and hydrogen aoms is equal or less than 45°).

Table S3. The atomic model subjected to energy minimization by DFT-D and restraints in the minimization

Segment	Number of residues	Substituted with Ala	Restraints
M3 (L253-C268)	16	D254, E255, E258, Q259, S261, K262, S265, L266	All Cα and L253Cδ1 atoms are spatially fixed.
M4 (A301-P312)	12		Backbone (N, Cα, and C) dihedral angles are fixed between V300C to V304N and between E/Q309C to A313N.
M5 (F760-I775)	16	R762, S766, V769, V773, C774	All Cα, F760Cε1/Cε2, Ile761Cδ, and Tyr763Cε1/Cε2 atoms are spatially fixed.
M6 (I788-G801)	14	I788, V790, Q791, W794, V798, T799	All Cα and D800Oδ1 atoms are spatially fixed.

* Altogether 58 (+8 capping) residues (consisting of 843 atoms, including hydrogens and protons, for the model with protonated Glu309) and 3 water molecules are included in the system.

Movie S1. Transition between native SERCA1a and E309Q mutant in E2. Viewed parallel to the membrane from two orthogonal directions. Color changes gradually as in Fig. 1.

Movie S2. Transition between E309Q in E2 and native SERCA1a in E1·Mg^{2+}. Viewed parallel to the membrane from two orthogonal directions. Color changes gradually as in Fig. 1.

Movie S3. Composite of three views showing the relationship among the changes in inclination of the M5 helix, the path of the unwound part of the M6 helix and orientation of the A-domain. The left panel shows details of the transmembrane region viewed nearly perpendicular to the membrane. The right panels show arrangement of the three cytoplasmic domains (top) and an entire molecule viewed parallel to the membrane (bottom).

References

1. Toyoshima C, et al. (2013) Crystal structures of the calcium pump and sarcolipin in the Mg^{2+}-bound E1 state. *Nature* 495:260-264.
2. Otwinowski Z, Minor W (1997) Processing of X-ray diffraction data collected in oscillation mode. *Methods Enzymol* 276:307-325.
3. Obara K, et al. (2005) Structural role of countertransport revealed in Ca^{2+} pump crystal structure in the absence of Ca^{2+}. *Proc Natl Acad Sci USA* 102:14489-14496.
4. Brünger AT, et al. (1998) Crystallography & NMR system: A new software suite for macromolecular structure determination. *Acta Crystallogr D Biol Crystallogr* 54:905-921.
5. Fabiola F, Bertram R, Korostelev A, Chapman MS (2002) An improved hydrogen bond potential: impact on medium resolution protein structures. *Protein Sci* 11:1415-1423.
6. Adams PD, et al. (2010) PHENIX: a comprehensive Python-based system for macromolecular structure solution. *Acta Crystallogr D Biol Crystallogr* 66:213-221.
7. Hayward S (1999) Structural principles governing domain motions in proteins. *Proteins* 36:425-435.
8. Kraulis PJ (1991) MOLSCRIPT: a program to produce both detailed and schematic plots of protein structures. *J Appl Crystallogr* 24:946-950.
9. Phillips JC, et al. (2005) Scalable molecular dynamics with NAMD. *J Comput Chem* 26:1781-1802.

10. Olsson MHM, Søndergaard CR, Rostkowski M, Jensen JH (2011) PROPKA3: Consistent Treatment of Internal and Surface Residues in Empirical pKa Predictions. *J Chem Theory Comput* 7:525-537.
11. Frisch MJ, et al. (2013) Gaussian 09, Revision D.01 (Gaussian, Inc. Wallingford, CT).
12. Hariharan PC, Pople JA (1974) Accuracy of AH n equilibrium geometries by single determinant molecular orbital theory. *Mol Phys* 27:209-214.
13. Becke AD (1993) Density-functional thermochemistry. III. The role of exact exchange. *J Chem Phys* 98:5648-5652.
14. Francl MM, et al. (1982) Self-consistent molecular orbital methods. XXIII. A polarization-type basis set for second-row elements. *J Chem Phys.* 77:3654-3665.
15. Frisch MJ, Pople JA, Binkley JS (1984) Self-consistent molecular orbital methods 25. Supplementary functions for Gaussian basis sets. *J Chem Phys.* 80:3265-3269.
16. Grimme S, Antony J, Ehrlich S, Krieg H (2010) A consistent and accurate ab initio parametrization of density functional dispersion correction (DFT-D) for the 94 elements H-Pu. *J Chem Phys* 132:154104.
17. Yanai T, Tew DP, Handy NC (2004) A new hybrid exchange–correlation functional using the Coulomb-attenuating method (CAM-B3LYP). *Chem Phys Lett* 393:51-57.
18. Pople JA, Head-Gordon M, Raghavachari K (1987) Quadratic configuration interaction. A general technique for determining electron correlation energies. *J Chem Phys* 87:5968-5975.
19. Purvis III GD, Bartlett RJ (1982) A full coupled-cluster singles and doubles model: The inclusion of disconnected triples. *J Chem Phys* 76:1910-1918.
20. Boys SF, Bernardi F (1970) The calculation of small molecular interactions by the differences of separate total energies. Some procedures with reduced errors. *Mol Phys* 19:553-566.
21. Simon S, Duran M, Dannenberg JJ (1996) How does basis set superposition error change the potential surfaces for hydrogen-bonded dimers? *J Chem Phys* 105:11024-11031.
22. Norimatsu Y, Hasegawa K, Shimizu N, & Toyoshima C (2017) Protein-phospholipid interplay revealed with crystals of a calcium pump. *Nature* 545:193-198.
23. Toyoshima C, Mizutani T (2004) Crystal structure of the calcium pump with a bound ATP analogue. *Nature* 430:529-535.
24. Raguimova ON, et al. (2018) Redistribution of SERCA calcium pump conformers during intracellular calcium signaling. *J Biol Chem* 293:10843-10856.
25. Ma H, Lewis D, Xu C, Inesi G, Toyoshima C (2005) Functional and structural roles of critical amino acids within the"N", "P", and "A" domains of the Ca^{2+} ATPase (SERCA) headpiece. *Biochemistry* 44:8090-8100.